Available online at www.sciencedirect.com
ScienceDirect
Computerized Medical Imaging and Graphics 32 (2008) 699–709
Computerized Medical Imaging and Graphics
www.elsevier.com/locate/compmedimag

Automated segmentation of mammary gland regions in non-contrast X-ray CT images

Xiangrong Zhou [a,*], Mingxu Han [a], Takeshi Hara [a], Hiroshi Fujita [a], Keiko Sugisaki [b], Huayue Chen [c], Gobert Lee [a], Ryujiro Yokoyama [d], Masayuki Kanematsu [b], Hiroaki Hoshi [e]

[a] *Department of Intelligent Image Information, Division of Regeneration and Advanced Medical Sciences, Graduate School of Medicine, Gifu University, Yanagito 1-1, Gifu 501-1194, Japan*
[b] *Department of Radiology, Gifu University Hospital, Yanagito 1-1, Gifu 501-1194, Japan*
[c] *Department of Anatomy, Division of Disease Control, Graduate School of Medicine, Gifu University, Yanagito 1-1, Gifu 501-1194, Japan*
[d] *Department of Radiology Service, Gifu University Hospital, Yanagito 1-1, Gifu 501-1194, Japan*
[e] *Department of Radiology, Division of Tumor Control, Graduate School of Medicine, Gifu University, Yanagito 1-1, Gifu 501-1194, Japan*

Received 28 December 2007; received in revised form 23 June 2008; accepted 15 August 2008

Abstract

The identification of mammary gland regions is a necessary processing step during the anatomical structure recognition of human body and can be expected to provide useful information for breast tumor diagnosis. This paper proposes a fully automated scheme for segmenting the mammary gland regions in non-contrast torso CT images. This scheme calculates the probability of each voxel belonging to the mammary gland or chest muscle in CT images as the reference of the segmentation, and decides the mammary gland regions based on CT number automatically. The probability is estimated from the location of the mammary glands and chest muscles in CT images. The location is investigated from a knowledge base that stores pre-recognized anatomical structures using a number of different CT scans. We applied this scheme to 66 patient cases (female, age: 20–80) and evaluated the accuracy by using the Jaccard similarity coefficient (JSC) between the segmented results and two gold standards that were generated manually by 2 medical experts independently for each CT case. The result showed that the mean value of the JSC score was 0.83 with the standard deviation of 0.09 for 66 CT cases. The proposed scheme was applied to investigate the breast density distributions in normal mammary gland regions so as to demonstrate the effect and usefulness of the proposed scheme.

Keywords: Segmentation; Mammary gland region; X-ray CT image; Probabilistic atlas

1. Introduction

Breast tumor detection is one of the most important tasks in clinical medicine. Breast imaging such as mammography, ultrasound, MR, and CT are widely used in breast lesion detection and/or characterization [1]. Currently, mammography is the most cost effective technique in breast cancer screening. However, mammograms are 2-D projection of objects, and cannot show 3-D structures in breast tissues that sometimes are required in diagnosis and surgical planning. On the other hand, the remarkable progress in multi-slice X-ray CT imaging enables the acquisition of the whole human torso in as little as 10–20 s. The volumetric torso CT scan contains details of all anatomical structures in the torso region, which enables the detection of lesions in different organs and tissue regions in the human torso. In principle, these CT images obtained including breast area may also be helpful in breast tumor risk prediction or detection in mammary gland regions.

Breast density is identified as an important risk factor for breast cancer development [2] and estimation of breast density in digital mammogram is also reported for the purpose of diagnosis [3]. Breast density may be measured using 3-D information in CT images. Here, the density (CT number) distribution is used as the breast density in mammary gland regions. The volume ratio of the dense tissue within the mammary gland regions have been suggested as a risk factor of breast cancer [4], so that the calculation of the volume ratio of breast dense tissues in CT images

* Corresponding author. Tel.: +81 58 230 6510; fax: +81 58 230 6514.
E-mail address: zxr@fjt.info.gifu-u.ac.jp (X. Zhou).

0895-6111/$ – see front matter © 2008 Elsevier Ltd. All rights reserved.
doi:10.1016/j.compmedimag.2008.08.007

Fig. 1. Examples of mammary gland regions in CT images from three female patient cases. White arrows show the locations of mammary gland region from left to right, 20, 56 and 70 years old.

is an important motivation and one of the useful applications of this research.

The segmentation of the mammary gland in CT images is a necessary primary processing step prior to the other processes such as breast density analysis. Because the mammary gland regions do not have a unique CT number distribution in CT images and the location of mammary gland regions is not stable compared with other organs, the automated segmentation of mammary gland in CT images is very difficult and cannot be solved using traditional segmentation methods based on CT numbers (such as gray-level thresholding, region growing) or shape-based method (such as snakes, active shape model) simply. Recently, the probabilistic atlas was reported as effective for solving the abdominal organ segmentation problem [5,6], however, the atlas for mammary gland regions has never been mentioned in the previous research works and automated segmentation of mammary gland regions in CT images has not been reported till now.

This research proposes an automated scheme to identify the mammary gland regions from the volumetric 3-D torso CT images. Some initial results of this research were reported in [7]. In this paper, we first describe the basic consideration of the method for mammary gland region segmentation and show the outline of the scheme. Next we provide details of the method, including the estimation of mammary gland locations and segmentation processes in Section 2. Experimental results are shown in Section 3, and discussions on mammary gland segmentation and breast density distributions in normal mammary gland regions are given in Section 4. Finally, conclusions are presented in Section 5.

2. Method

2.1. Mammary gland regions in CT images

The breasts consist of mammary gland with the associated skin and connected tissues. The mammary glands are modified sweat glands in the superficial fascia anterior to the pectoral muscles and anterior thoracic wall in human anatomy. The mammary glands consist of a series of ducts and associated secretory lobules. These converge to from 15 to 20 lactiferous, which open independently onto the nipple. The nipple is surrounded by a circular pigmented area of skin termed the areola [8]. On 3-D CT images, mammary gland regions appear as mass regions with an irregular shape and a density (CT number) distribution similar to the chest muscles. The volume and density of the mammary gland regions change greatly depending on the individual variation and the age of the patients as shown in Fig. 1.

2.2. Outline of segmenting mammary gland regions

The approach for segmenting mammary gland regions includes 3 processing steps as shown in Fig. 2. Firstly, some key anatomical structures in a target CT case are recognized automatically and used as the reference to present the coordinate space of the patient. And then, the range and location of the mammary gland regions under the coordinate space is estimated based on a knowledge base. Referring to the range and location of mammary gland regions estimated in the previous step, a density (CT number) based segmentation method is used to decide the mammary gland regions voxel-by-voxel preciously in CT images.

Estimation of the location of mammary gland regions for a specific CT case is the most important part of this approach. A knowledge base including a number of pre-recognized anatomical structures and mammary gland locations are constructed previously to support the estimation process. By registering and deforming the key anatomical structures in different CT images, mammary gland locations in the different patient cases stored in the knowledge base are integrated and mapped into a spe-

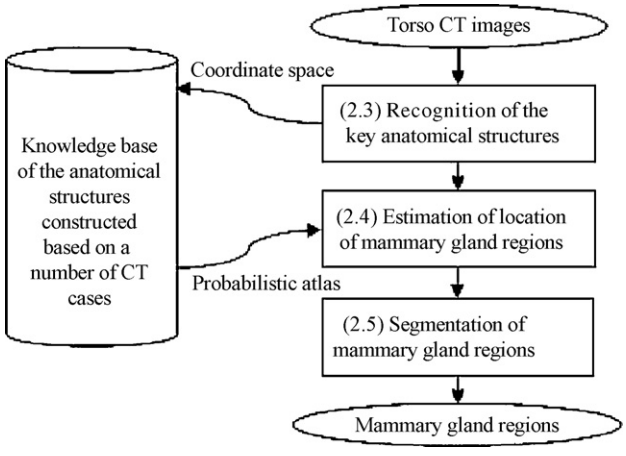

Fig. 2. Processing flow of segmenting the mammary gland regions from CT images.

cific CT case as the reference. The details of each processing step of segmentation [Fig. 2] are described in the following sections.

2.3. Recognition of the key anatomical structures

The purpose of this step is to extract some landmarks that have high spatial relations with the locations of mammary gland regions in CT images. Such landmarks are used as the coordinate space to present the locations of mammary gland regions in different patients. The body surface, surface of thoracic cavity, nipple, subcostal plane, and jugular notch are regarded as the key anatomical structures for landmark selection. The details of the recognition process for such key anatomical structures are described in following sections.

2.3.1. Extraction of body surface

The whole region in torso CT images is divided into 4 parts (air, fat, muscle and organ, and bone) which have the unique density distributions that can be distinguished from the density (CT number) histogram of CT images [9]. A gray-level thresholding process is used for the region division. The optimized threshold values for segmenting each target region are estimated dynamically from the input images using a histogram analysis [10]. A connected component processing including a combination of small region deletion and a binary morphological operator is used to refine the extracted regions. Then, the body surface is identified finally by a 3-D contour tracing method using contour between the extracted human tissue and air reigns outside of human body [10].

2.3.2. Extraction of thoracic cavity surface

The thoracic cavity region is surrounded by the bone frame and closed by the diaphragm. The thoracic cavity region is extracted using a ball-kernel based region growing process limited by the spatial position of bone frame within the chest region [9] and diaphragm is extracted based on a thin-plate model [11]. The parameter of the ball kernel is calculated and decided automatically from the size of circumscribed rectangle of bone frame for each patient case, respectively [9]. The surface of the extracted thoracic cavity region is identified by the 3-D contour tracing method used in Section 2.3.1.

2.3.3. Extraction of nipple locations

The nipples are the most important landmarks showing the positions of mammary gland regions. The positions of nipples are identified based on a shape analysis on body surface using the following three processing steps: (i) the 3-D curvatures of the body surface extracted in Section 2.3.1 are calculated and the convex points are found out as the candidates of the nipples; (ii) the 3-D body surface [Fig. 3(a)] is deformed to a 2-D thin-plate [Fig. 3(b)] by a body stretching process [12] and a range map [Fig. 3(c)] is generated to show the statistical nipple locations based on a knowledge base (a number of pre-recognized anatomical structures of human torso). Within range map [ellipse line in Fig. 3(c)], we reduce the false positives of the nipple candidates identified using the curvatures of body surfaces in step 1. (iii) The nipple position on right (or left) side of human body surface is decided respectively within the range map generated in step 2 by searching the nipple candidates p that has the maximum ratio

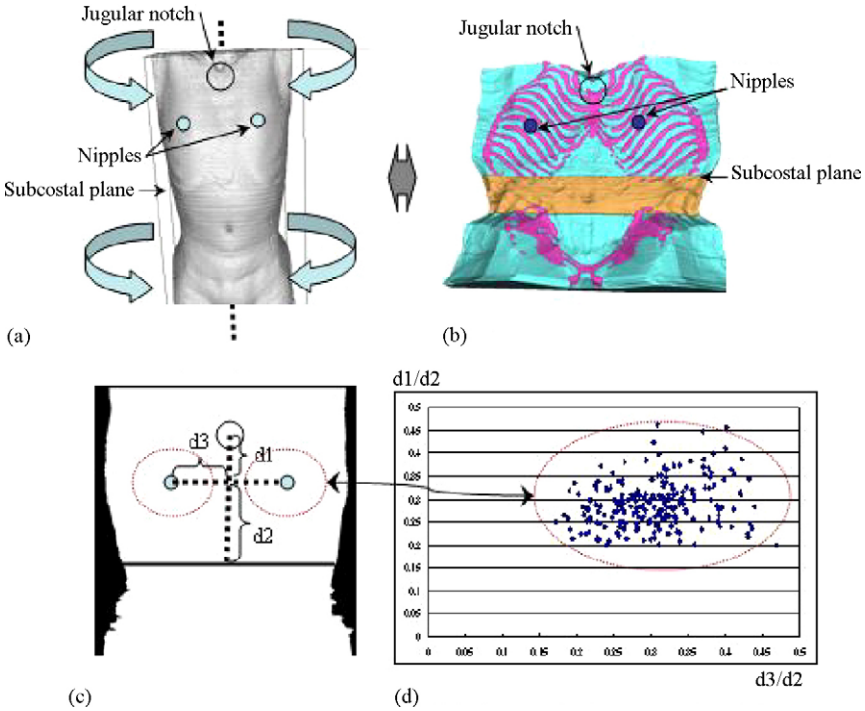

Fig. 3. Estimation of nipple locations based on body stretching image. (a) Body surface, (b) body stretching image, (c) body surface in stretching image, and (d) statistic nipples locations on (c) of 105 CT cases.

$A(p)$ defined in the following equation.

$$A(p) = \frac{S1}{S2}, \quad (1)$$

where $S1$ and $S2$ are volume of the muscles inside a ball with the center p and radius $d = 10$ (voxels) and volume of the human tissues inside a ball with the center p and radius $d = 10$ (voxels), respectively.

2.3.4. Extraction of subcostal plane and jugular notch

Subcostal plane and jugular notch are used as upper and lower boundaries for searching the location of mammary gland regions. For identifying the subcostal plane, we calculate the areas of the circumscribed box of bone region slice-by-slice, and decide the position of subcostal plane by searching the slice number of CT images that has a biggest decrease in area of the circumscribed box. For extracting the jugular notch location, the relationship between the airway of trachea and bone regions is used. The airway of trachea is extracted based on the air region inside of human body using a 3-D region growing method [10]. The jugular notch location is extracted using the following processing steps.The key anatomical structures

(1) Extract the axis line of the airway of trachea using a 3-D thinning algorithm.
(2) Extract a profile of CT number in sagittal direction start from the axis line of airway and end at the anterior surface of human body slice-by-slice, respectively.
(3) Integrate the profile in each CT slice to generate a sagittal curve plane through the axis line of the airway.
(4) Analyze the location of bone region in the sagittal curve plane and consider the voxel in bone region that is nearest to the neck (the first slice of CT image) as the jugular notch.

extracted in this section are used as the landmarks to show the spatial coordinates space in CT images that are necessary during the inter-patient registration required before the estimation of mammary gland locations.

2.4. Estimation of location of mammary gland regions

A knowledge base is constructed to support the estimation of mammary gland locations in a specific CT case. A number of the torso CT cases and corresponding anatomical structures are collected and stored in the knowledge base. The mammary gland regions in all cases are also pre-segmented and instructed by a radiologist (K.S.) and an anatomist (H.C.) independently. For estimating the location of mammary gland regions in an input CT case, we firstly get the coordinate space of the patient in CT images by extracting the key anatomical structures (described in Section 2.3), and then, arrange all the CT images in the knowledge base to the coordinate space of the input CT image and integrate the location and range of the mammary gland regions to generate probabilistic atlases that show the existences of mammary gland regions. The same method is also used to generate the probabilistic atlases for chest muscle regions in the input CT case. We describe the details in the following sections.

2.4.1. Arranging the locations of mammary gland regions in different CT cases

A coordinate space is defined based on the location of the key anatomical structures in each CT case. A point distribution model (PDM, a number of sampling points selected from the key anatomical structures) is used as the coordinate space to express the location of mammary gland region. The points of PDM are selected from the nipple (2 points); body surface (238 points) and thoracic cavity surface (160 points) [Fig. 4(a)]. The points on the body surface are selected from the crossing points of a grid with the equal interval inside of the 8 sections $A_{i,j}$ on the body surface from the stretching image as shown in [Fig. 4(b)]. The sections are decided by the locations between left and right nipples and jugular notch to subcostal plane [Fig. 4(b)]. The points on the surface of the thoracic cavity are also selected based on the same method [Fig. 4(c)]. Using the correspondence between the different PDMs, the mammary gland regions in different CT cases are arranged to the same coordinate space.

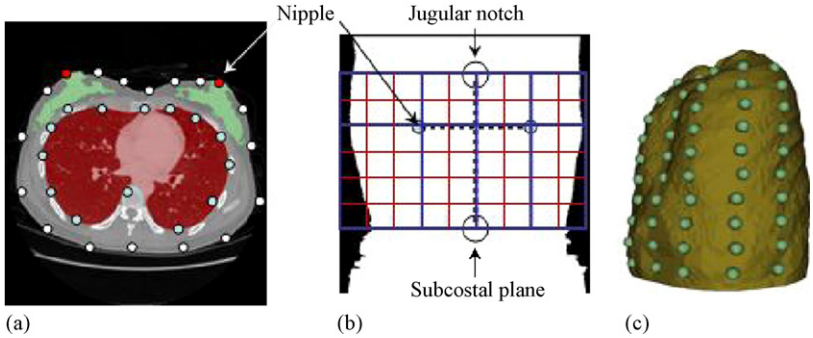

Fig. 4. A point distribution model that shows the anatomical structure surrounding the mammary gland regions: (a) points on a slice of CT images, (b) point selections on body surface, and (c) points on surface of thoracic cavity.

2.4.2. Estimating the location of mammary gland region in a specific CT case

The PDM of the patient in the input CT case is identified firstly and used as the standard coordinate space. Then, all the anatomical structures stored in the knowledge base are normalized by moving each point in PDM to the corresponding position in the standard coordinate space and deforming the whole mammary gland regions in each CT case based on thin-plate splines (TPS) algorithm [13], respectively. After normalizing the anatomical structure in each case stored in knowledge base, we investigate appearances of the mammary gland regions and chest muscle regions under the standard coordinate space and generate the likelihoods of mammary gland regions and chest muscle regions in each voxel position respectively by the following algorithms.

$$\text{Prob.}_t(x, y, z) = \frac{\sum_{i=1}^{N} \text{Voting}_i(x, y, z, t)}{N} \quad (2)$$

N: total number of CT cases in knowledge base.
x, y, z: voxel indexes of an input CT case.
i: number of CT case.
$\text{Voting}_i(x, y, z, t) =$

1 : the voxel at (x, y, z) inside the target region t in CT case i.

0 : the voxel at (x, y, z) outside the target region t in CT case i.

We call those likelihood images as probabilistic atlases [Fig. 5(a)] that show the likelihood of the mammary or muscle region in the input CT image [Fig. 5(b)] based on the anatomical knowledge.

The contour under the condition ($\text{Prob.}_{\text{Mam}} = \text{Prob.}_{\text{Muscle}}$) is selected as the initial decision boundary in CT images [Fig. 5(c)]. Based on this decision boundary, the region R_{mam} where each voxel inside of the R_{mam} satisfied a condition ($\text{Prob.}_{\text{Mam}} > \text{Prob.}_{\text{Muscle}}$) is regarded as the location of mammary gland region [we call it as mask image in Fig. 5(d)].

2.5. Segmentation of mammary gland regions

A density-based method is used for segmenting the mammary gland regions. The density (CT number) range is decided for the input cases based on the estimated location of mammary gland regions. Finally, a combination of density thresholding and connected-component labeling is used to segment mammary gland regions from CT images.

Two kinds of tissues (mammary gland and fat) are inside of the mask image obtained in Section 2.4. The distribution of each of the tissue regions is approximated as a normal distribution N (μ, σ). Because the volume of the fat is quite larger than that of the mammary gland within the range of the mask image, we only calculate the CT number distribution of the fat region by estimating the normal distribution N (μ, σ) of fat tissues. In fact, the CT number that has the maximum (peak value) of the histogram is selected as the μ and the HWHM (half width at half maximum) is used to approximate σ as shown in Fig. 6. The CT numbers that are greater than $\text{Th} = \mu + 3\sigma$ are regarded as the density range of the mammary gland regions in the CT images.

With the estimated location and density range of the mammary gland regions in CT image, the mammary gland regions are decided by selecting the voxels P that satisfied the following conditions: (1) the CT number of the P in CT images is larger than Th, and (2) the location of P in mask image is inside of the mammary gland regions. Finally, the segmented mammary gland regions are refined by a connected-component processing [Fig. 5(e)].

2.6. Density analysis of mammary gland regions

The histogram of the segmented mammary gland regions is used in density analysis. Some typical density (CT number) distributions in both left and right mammary gland regions from three patient cases under the different age stages are shown in Fig. 7. The mammary gland regions can be divided to fatty tissue and dense tissue that show the different CT numbers. The volume ratio of the dense tissue within the mammary gland regions is suggested as a feature of histogram. A density thresholding method is used to separate the fatty tissue and dense tissue automatically. Because the CT number distribution in the chest muscle regions is similar to the dense tissues in mammary gland regions, the minimum CT number of the chest muscle regions in the same CT image is used as a substitute threshold value for segmenting the dense tissues. This idea was also used in determining the dense breast tissues in mammography [4]. The volume ratio of the dense tissue regions and total mammary gland regions is regarded as the final output of breast density analysis.

3. Experimental results

Non-contrast CT scans of 66 females were used for mammary gland segmentation in this study. The age of the patients ranges from 20 to 80 years old (20s: 4 cases; 30s: 5 cases; 40s: 6 cases; 50s: 17 cases; 60s: 13 cases; 70s: 17 cases; 80s: 4 cases) and centers around 50–70 years old. No abnormality about mammary gland regions was reported in each patient case. Each CT image has an isotopic spatial resolution of about 0.6 mm in voxel size and density (CT number) resolution of 12 bits. The voxel size of each CT image was converted 1.2 mm in the experiment.

The gold standards of mammary gland regions were identified manually using an interactive user interface. This interface provided a semi-automatic tool to generate the candidate regions of mammary glands, and then the candidate regions were validated and refined manually slice-by-slice by a human operator. For each case, two gold standards of mammary gland regions were generated independently by Author K.S. (a radiologist specialized in breast cancer) and Author H.C. (a medical doctor specialized in anatomy). The gold standards (264 regions

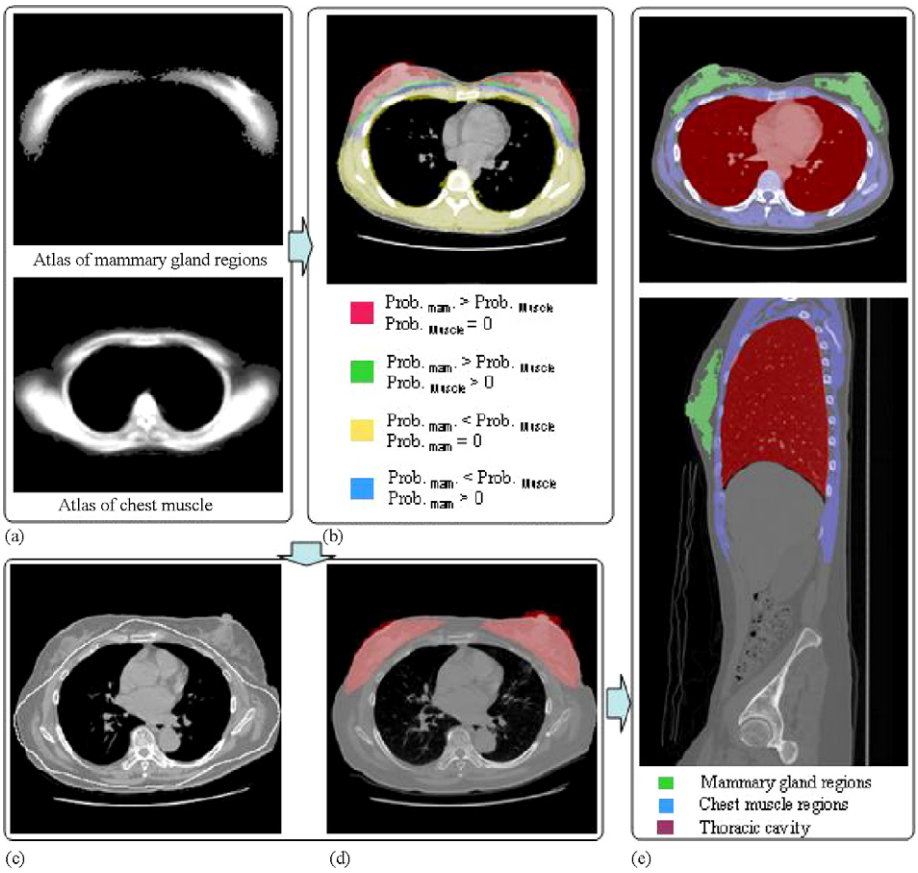

Fig. 5. Segmentation of mammary gland regions. (a) Probabilistic atlases, (b) probabilistic atlases over the CT images, (c) decision boundary between mammary gland regions and chest muscles, (d) mask images (red regions) of the mammary gland regions, and (e) segmentation results of mammary glands (1 axial slice and 1 sagittal slices). (For interpretation of the references to color in this figure legend, the reader is referred to the web version of the article.)

including left and right mammary gland regions in 66 cases, by 2 independent manual inputs) were separated into two groups (GS1 generated by Author K.S. and GS2 generated by Author H.C.) and used for atlas construction and performance evaluation.

The proposed scheme was applied to 66 CT cases to segment the left and right mammary gland regions. Leave-one-out cross-validation (using 65 cases to construct an atlas and segment the mammary gland regions based on the atlas from the remaining 1 case) was used in the experiment for performance evaluation. The accuracy was evaluated by using Jaccard similarity coefficient (JSC) between the segmented mammary gland regions and two corresponding gold standards (GS1 and GS2). The JSC scores of each case are shown in Fig. 8. We confirmed that the mean values of the JSC scores were 0.825 for GS1 and 0.828 for GS2 with standard deviations of 0.09 (GS1) and 0.09 (GS2) for 66 cases.

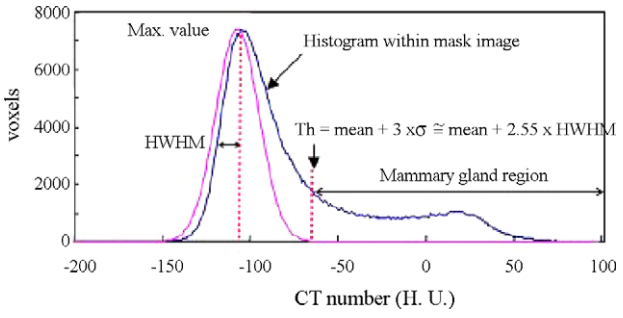

Fig. 6. Threshold value (Th) decision for segmenting the mammary gland region.

Some experimental results that had the higher scores of JSC are shown in Fig. 9, and some results that had the lower scores of JSC are also illustrated in Fig. 10.A typical CT slice including the main part of mammary gland regions for each patient case are shown in Figs. 9 and 10. The gold standards (GS1) and automated extraction results of mammary gland regions on the same CT slices are also illustrated for detailed comparison in Figs. 9 and 10. A 3-D view of whole mammary regions (both gold-standard and extracted result) are also presented in Figs. 9 and 10, and the surfaces of muscles are shown in the same image as well using different colors as a reference.

The density of mammary gland regions in CT images was analyzed by calculating the volume ratio of the dense tissue within the mammary gland regions. Fig. 11 shows the volume ratios of the dense tissue for 66 CT cases based on the segmented mammary gland regions. The same ratio values calculated from

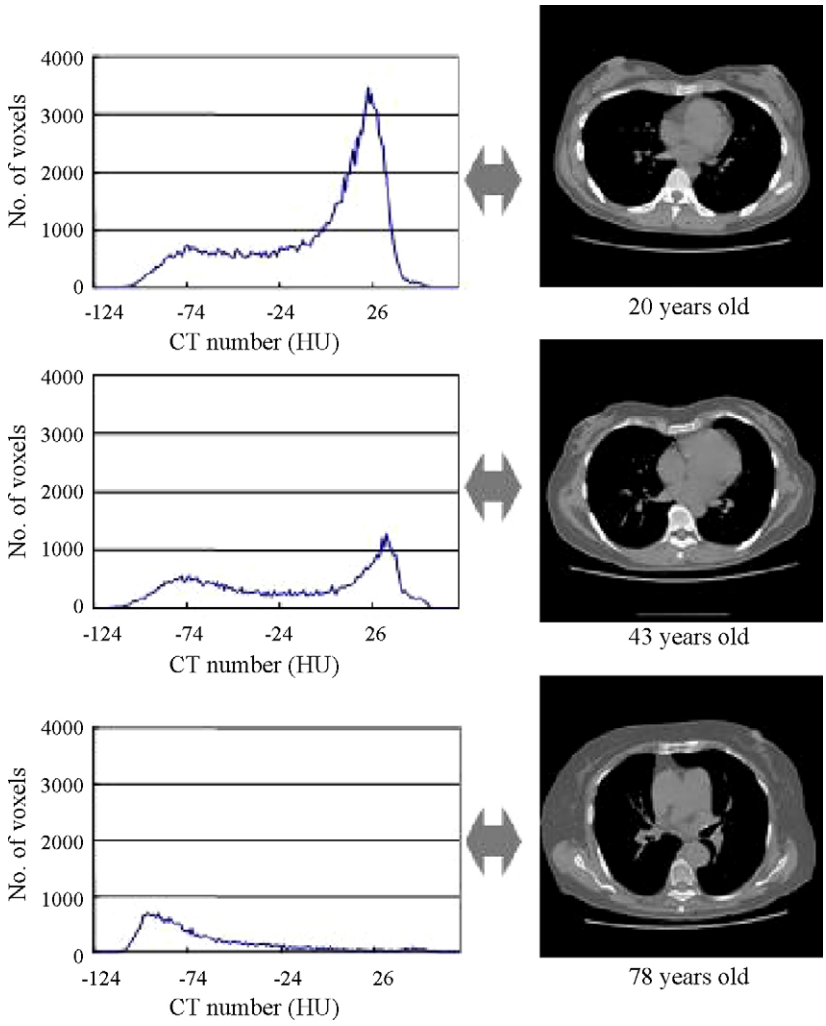

Fig. 7. Variation of the density distribution within mammary gland regions with the age increases from 20s to 70s. Histogram of mammary gland region in CT images on the left and a corresponding slice of CT images on the right.

the gold standard of mammary gland regions are also shown in Figs. 11 (GS1) and 12 (GS2) for the accuracy evaluation. The error (absolute difference between 2 calculated volume ratios in the same CT case) had a mean value of 2.00 % with a standard deviation of 2.25 for GS1 and 2.38 % with a standard deviation of 3.24 for GS2, using 66 CT cases.

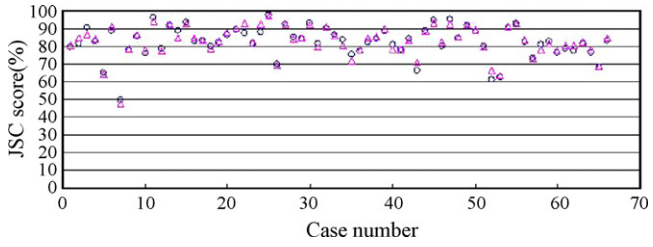

Fig. 8. Jaccard similarity coefficient (JSC) scores between the segmentation results of mammary gland regions, which were determined with two different sets of gold standards generated by 2 medical experts using 66 CT cases. Δ: JSC scores using the gold standards 1 (GS1). ◯: JSC scores using the gold standards 2 (GS2).

4. Discussion

We compared the gold standards that were independently generated by 2 medical experts. The JSC scores between two gold standards for each CT case ranged from 0.96857 to 0.9969 as shown in Fig. 13. The mean value of JSC was 0.994 with a standard deviation of 0.007 for 66 CT cases. This result showed the good convergence of the gold standards of mammary gland regions from the different experts and verified the reliability of the gold standards that were used for the accuracy evaluation in our experiments.

The experimental results showed that the majority of mammary gland regions in each CT case were extracted successfully by the proposed scheme. However, some over-extracted regions that occurred as the misclassification between chest muscle and mammary gland regions were observed in some CT cases (Fig. 10). Two sets of the gold standards were used to evaluate the accuracy independently. The JSC scores between the segmentation results and GS1 ranged from 0.976 to 0.494 and had a mean value of 0.825 with the standard deviation of 0.09. The

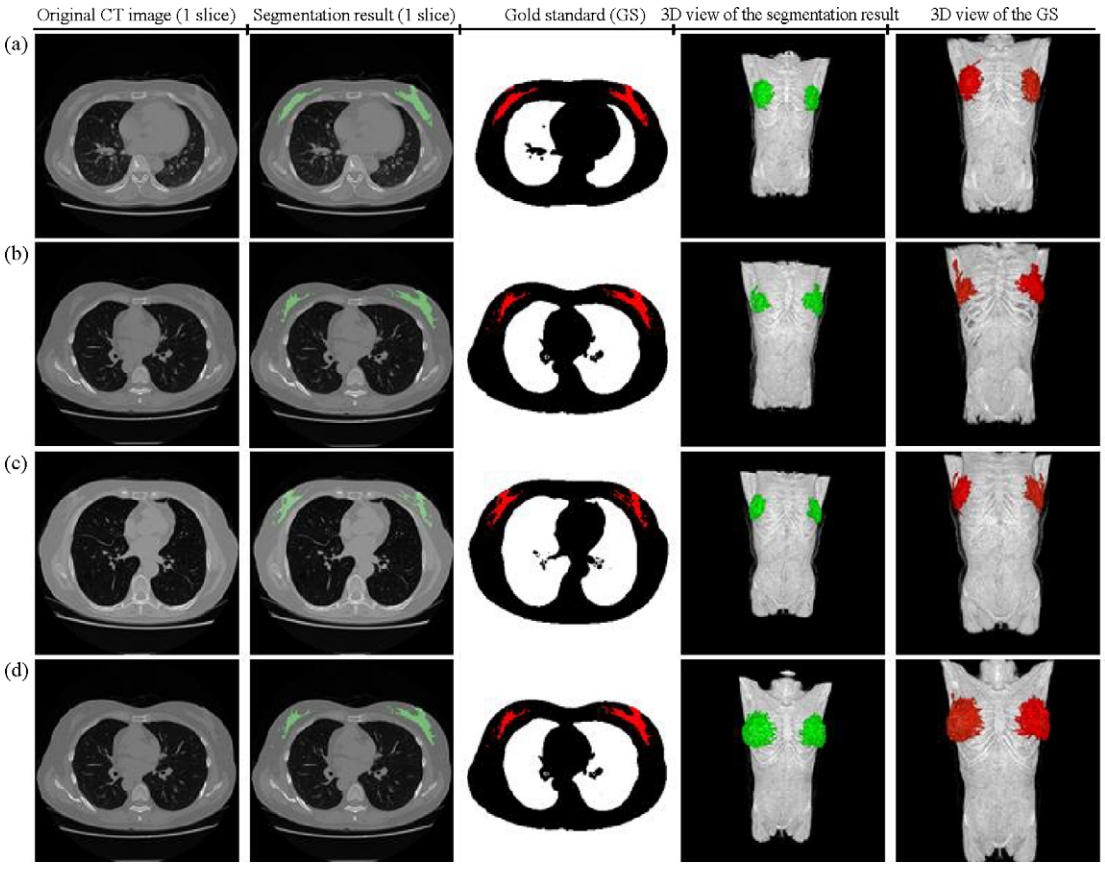

Fig. 9. Four examples of segmentation results (green) and gold standards (red) of mammary gland regions with high evaluation scores (a–d: the patient age is 53, 53, 70, and 34 years old, and the coincidence ratio between segmentation result and gold standard (GS1) is 0.976, 0.965, 0.954, and 0.937, respectively). (For interpretation of the references to color in this figure legend, the reader is referred to the web version of the article.)

JSC scores between the segmentation results and GS2 ranged from 0.971 to 0.476 and had a mean value of 0.828 with the standard deviation of 0.09 [refer to Fig. 8]. The experimental results showed that accuracy of the segmentation results was not changed largely under 2 independent evaluations by 2 medical doctors. The segmentation results also showed the robustness of the proposed scheme for patients of different age groups.

The probabilistic atlas used in this study showed usefulness and robustness for identifying the location of mammary gland regions. Our atlas construction method was similar to some previous research works that have been presented for segmenting the abdominal organs in CT images [5,6]. However, comparing to the abdominal organ regions, the volume, anatomical location and shape of mammary gland regions in different CT images showed larger variation. Constructing atlases for mammary gland regions was more challenging and required more information of anatomical structures during the atlas construction as well as atlas application. The experimental results showed that the locations of nipple, surface of body, surface of thoracic cavity, subcostal plane and jugular notch were effective in guiding the atlas construction and application successfully and such anatomical structures could be identified automatically in each case by the proposed scheme.

Further information such as the anatomical structure of skeletal muscle system will be very helpful during the mammary gland region segmentation. However, recognizing the skeletal muscle system was also challenging and has not been solved completely yet [14]. Recently, a scheme was reported to recognize some anatomical structures for radiotherapy planning using thoracic and pelvis CT images [15]. Implicit anatomical knowledge and organ-specific segmentation strategies were used in segmentation. However, this scheme did not show the capability for mammary gland regions identification in CT images.

Constructing atlases for mammary gland region and chest muscle based on 65 CT cases required about 8 h using a computer (CPU: AMD Opteron(tm) Processor 2.39 GHz; Memory: 8 GB). After the atlases were constructed, the computation cost of the mammary gland region segmentation was about 46 s/CT case. (Computing time ranged from 42 to 55 s according to the different CT cases that included 425–552 slices/CT case.)

The segmentation results were used to analyze the density of mammary gland regions by calculating the volume ratio of the dense tissue within mammary gland regions. This result showed that the accuracy of the volume ratio obtained using the automated segmentation is comparable with the results based on the mammary gland regions extracted manually by the medical experts [Figs. 11 and 12]. We also investigated the distribution (mean value and standard deviation) of the volume ratios under the different age groups and the results are illustrated in Figs. 14 and 15. The results shows that the density distribution

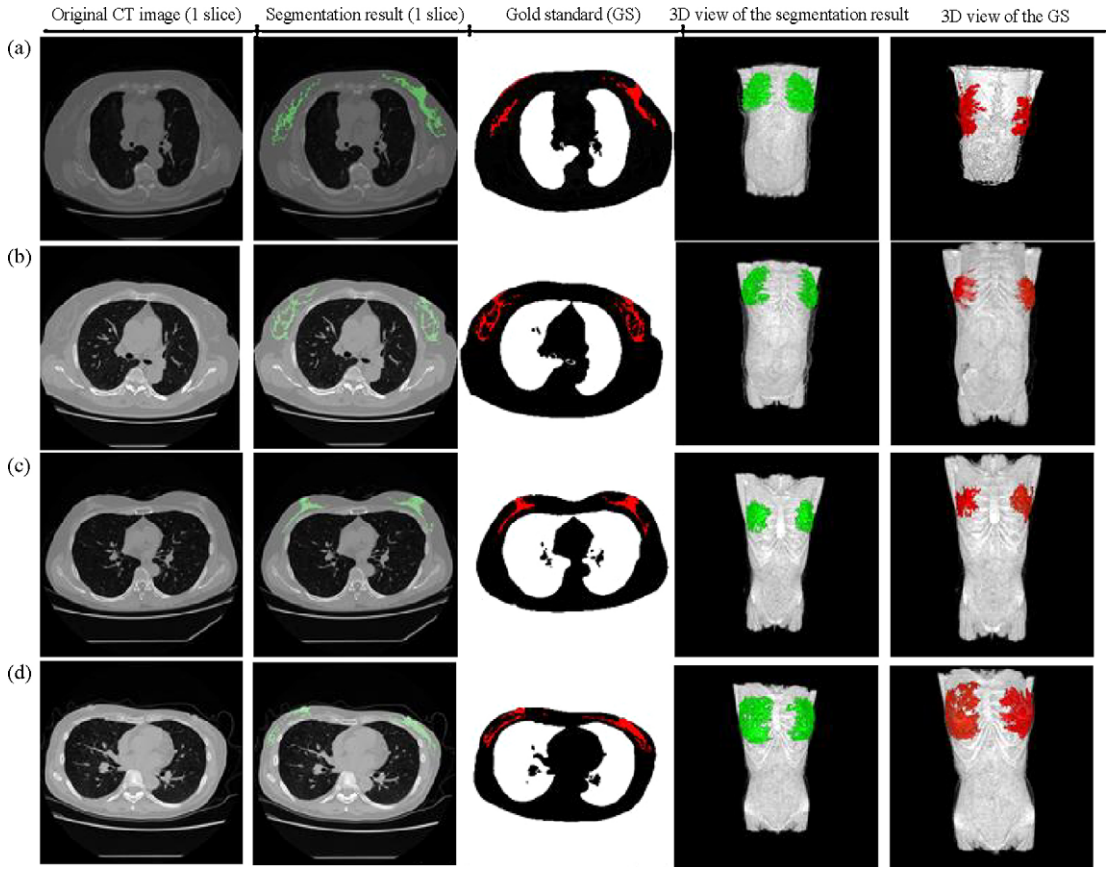

Fig. 10. Four examples of segmentation results (green) and gold standards (red) of mammary gland regions with low evaluation scores (a–d: the patient age is 77, 53, 45, and 52 years old, and the coincidence ratio between segmentation result and gold standard (GS1) is 0.733, 0.700, 0.625, and 0.494, respectively). (For interpretation of the references to color in this figure legend, the reader is referred to the web version of the article.)

of mammary gland regions has two significant changes at 30s and 70s, and varies in a large range in each of the age stages. We found that the automated calculation based on the proposed scheme [Figs. 14(b) and 15(b)] was quite close to that calculated based on the manual extraction results [Figs. 14(a) and 15(a)]; the error of mean value between the different age groups was less than 3.3%. The experimental results showed the potential and efficiency of the proposed scheme for investigating the features of mammary gland regions. Such investigation always uses a large number of CT images, the manual segmentation and calculation are time consuming and sometimes impossible. The proposed scheme can act as an automated tool for investigating

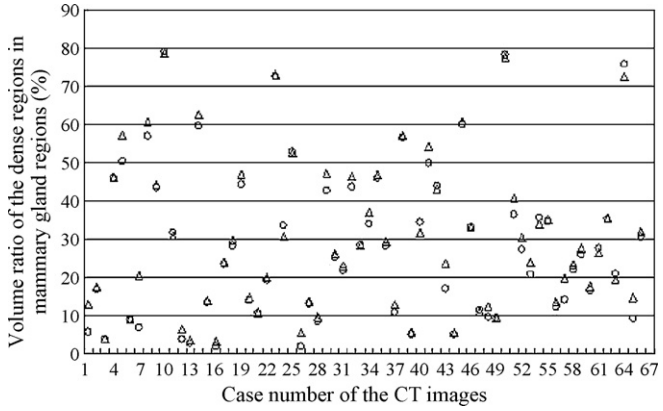

Fig. 11. The volume ratios of the dense regions in mammary gland regions based on the gold standard (GS1) and segmented mammary gland regions (the error between 2 calculated volume ratios had a mean value of 2.00% with a standard deviation of 2.25). Δ: Ratios calculated from the automated segmentation results. ◯: Ratios calculated from the gold standards (GS1).

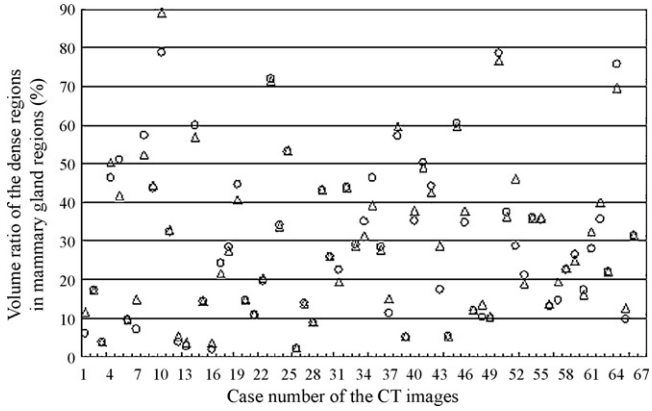

Fig. 12. The volume ratios of the dense regions in mammary gland regions based on the gold standard (GS2) and segmented mammary gland regions (the error between 2 calculated volume ratios had a mean value of 2.38% with a standard deviation of 3.24). Δ: Ratios calculated from the automated segmentation results. ◯: Ratios calculated from the gold standards (GS2).

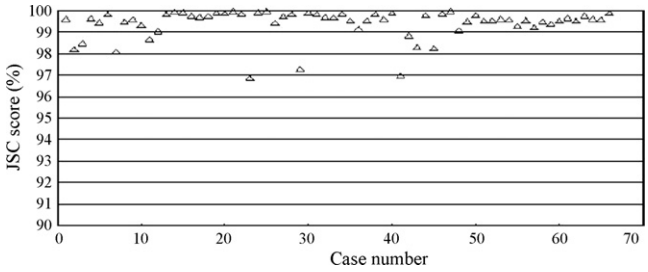

Fig. 13. Jaccard similarity coefficient (JSC) scores between two sets of gold standards of the mammary gland regions that were generated independently by 2 medical experts using 66 CT cases.

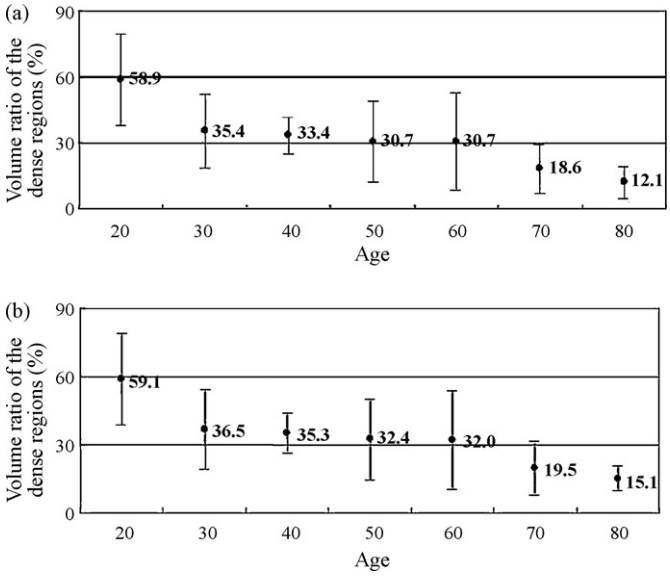

Fig. 14. Variety (mean value ± S.D.) of volume ratios of the dense regions in mammary gland regions under the different age stages. Calculation results for (a) using the gold standard (GS1) and (b) using automated segmentation results of mammary gland regions based on GS1.

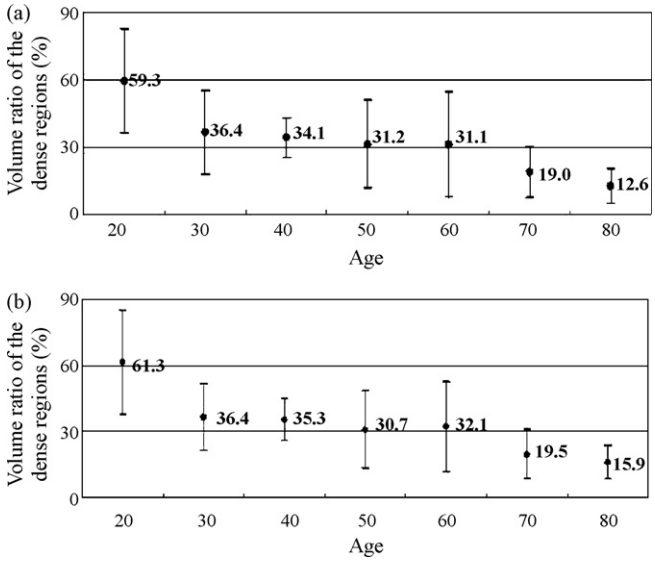

Fig. 15. Variety (mean value ± S.D.) of volume ratios of the dense regions in mammary gland regions under the different age stages. Calculation results for (a) using the gold standard (GS2) and (b) using automated segmentation results of mammary gland regions based on GS2.

features of mammary gland region in CT images quickly and efficiently.

The investigation of the normal situation of the human body, as well as the lesion recognition during the development of computer-aided diagnosis (CAD) system is important. We are developing a new CAD system that aims at normal anatomical structure recognition using torso CT images [16], which is a solution for multi-disease detections and multi-organ diagnosis required by a future CAD research project [17]. The proposed scheme in this paper is a part of this type of CAD systems and the investigation results of the mammary gland regions will be applied to breast cancer diagnosis in the future.

5. Conclusion

We developed a fully automated scheme for segmenting the mammary gland regions in non-contrast X-ray CT images. The proposed method, using the probabilistic atlas and density (CT number) estimation, was efficient and robust for mammary gland segmentation. We confirmed that our scheme could extract the mammary gland regions in 66 torso CT scans successfully. Based on the segmentation results, the automated measurement for volume ratio of the dense tissues in mammary gland regions was developed and practiced. The experimental results showed the possibility and usefulness of breast dense tissue measurement in CT images and that may be useful for risk analysis of the breast tumor at the initial stage.

Acknowledgements

The authors would like to thank Dr. T. Matsubara and members of the Fujita Laboratory for their valuable discussions. This research was supported in part by research grants of Grant-in-Aid for Scientific Research, in part by Ministry of Health, Labour, and Welfare under a Grant-In-Aid for Cancer Research, and in part by the Knowledge Cluster Initiative of the MEXT, Japanese Government.

References

[1] Kopans DB. Breast imaging. Philadelphia: J.B. Lippincott Company; 1989.
[2] Byrne C, Schairer C, Wolfe J, Parekh N, Salane M, Brinton LA, et al. Mammographic features and breast cancer risk: effects with time, age, and menopause status. J Natl Cancer Inst 1995;77(21):1622–9.
[3] Engeland SV, Snoeren PR, Huisman H, Boetes C, Karssemeijer N. Volumetric breast density estimation from full-field digital mammograms. IEEE Trans Med Imag 2006;25(3):273–82.
[4] Nagata C, Matsubara T, Fujita H, Nagao Y, Shibuya C, Kashiki Y, et al. Associations of mammographic density with dietary factors in Japanese women. Cancer Epidemiol Biomark Prev 2005;14(12):2877–80.
[5] Park H, Bland PH, Meyer CR. Construction of an abdominal probabilistic atlas and its application in segmentation. IEEE Trans Med Imag 2003;22(4):483–92.
[6] Shimizu A, Ohno R, Ikegami T, Kobatake H, Nawano S, Smutek D. Segmentation of multiple organ in non-contrast 3D abdominal CT images. Int J CARS 2007;2:135–42.
[7] Zhou X, Kan M, Hara T, Fujita H, Sugisaki K, Yokoyama R, et al. Automated segmentation of mammary gland regions in non-contrast CT images based on probabilistic atlas. Proc SPIE Med Imag 2007: Image Process 2007;6512, 65123O-1-8.

[8] Drake RL, Vogl W, Mitchell AWM. Gray's anatomy for students. Philadelphia: Elsevier; 2005.
[9] Zhou X, Hara T, Fujita H, Yokoyama R, Kiryu T, Kanematsu M, et al. Preliminary study for automated recognition of anatomical structure from torso CT images. In Proceedings of the 2005 IEEE engineering in medicine and biology 27th annual conference, paper#340; 2005.
[10] Zhou X, Hayashi T, Hara T, Fujita H, Yokoyama R, Kiryu T, et al. Automatic segmentation and recognition of anatomical lung structures from high-resolution chest CT images. Comput Med Imag Graph 2006;30(5):299–313.
[11] Zhou X, Ninomiya H, Hara T, Fujita H, Yokoyama R, Chen H, et al. Automated estimation of the upper surface of the diaphragm in 3-D CT images. IEEE Trans Biomed Eng 2008;55(1):351–3.
[12] Zhou X, Kamiya H, Hara T, Fujita H, Chen H, Yokoyama R, et al. Automated segmentation and recognition of abdominal wall muscles in X-ray torso CT images and its application in abdominal CAD. Int J Comput Assist Radiol Surg 2007;2(Suppl. 1):s388–90.
[13] Bookstein FL. Principal warps: thin-plate splines and the decomposition of deformations. IEEE Trans Pattern Anal Mach Intell 1989;11(6):567–85.
[14] Zhou X, Kamiya N, Hara T, Fujita H, Chen H, Yokoyama R, et al. Automated segmentation and recognition of abdominal wall muscles in X-ray torso CT images and its application in abdominal CAD. Int J Comput Assist Radiol Surg 2007;2(Suppl. 1):S388–90.
[15] Haas B, Coradi T, Scholz M, Kunz P, Huber M, Oppitz L Andre, et al. Automatic segmentation of thoracic and pelvic CT images for radiotherapy planning using implicit anatomic knowledge and organ-specific segmentation strategies. Phys Med Biol 2008;53:1751–71.
[16] Fujita H, Zhou X, Hara T, Yokoyama R, Kondo H, Kiryu T, et al. Digital representation of diagnostic knowledge: anatomical structures in human torso region. In: Proceedings of the second international symposium on intelligent assistance in diagnosis of multi-dimensional medical images. 2006. p. 50–6.
[17] Kobatake H. Future CAD in multi-dimensional medical images: project on multi-organ, multi-disease CAD system. Comput Med Imag Graph 2007;31(4–5):258–66.

Xiangrong Zhou received the MS and PhD degree in information engineering from Nagoya University, Japan in 1997 and 2000, respectively. From 2000 to 2002, he continued his research in medical image processing as a postdoctoral researcher at Gifu University, and currently, he is an assistant professor of Graduate School of Medicine, Gifu University, Japan. His research interests include medical image analysis, medical image visualization and pattern recognition.

Mingxu Han received the BS degree in Department of Information Science Faculty of Engineering in 2006 from Gifu University. Currently, he is a MS candidate in Graduate School of Medicine of Gifu University, Japan. His research interests include medical image processing and computer-aided diagnosis.

Takeshi Hara received the MS and PhD degrees in electrical engineering from Gifu University, Japan, in 1994 and 2000, respectively. He is currently an associate professor in the Department of Intelligent Image Information, Graduate School of Medicine, Gifu University, Japan. His research interests include computer network, medical image processing and pattern recognition.

Hiroshi Fujita received the BS and MS degrees in electrical engineering from Gifu University, Japan, in 1976 and 1978, respectively, and PhD degree from Nagoya University in 1983. He was a research associate at University of Chicago, USA, from 1983 to 1986. He is currently a chairman and a professor in the Department of Intelligent Image Information, Graduate School of Medicine, Gifu University, Japan. His research interests include computer-aided diagnosis system, image analysis and processing, and image evaluation in medicine.

Keiko Sugisaki is currently a radiologist majored in breast imaging in Gifu University Hospital.

Huayue Chen received MD degree and PhD degree at Gifu University, Japan, in 1992. He served as an associate professor in the Department of Anatomy, Zhejiang University School of Medicine from 1993 to 1995. He is currently an instructor of Graduate School of Medicine, Gifu University. His research interests include medical image analysis.

Gobert Lee received the MSc degree in applied physics from the Royal Melbourne Institute of Technology, Melbourne, Australia, in 1995 and the PhD degree from the Flinders University, Adelaide, Australia, in 2003. She was a research associate at the Flinders University from 2002 to 2004 and was awarded a Post-doctoral Research Fellowship by the Japan Society for the promotion of Science. She is currently a research associate at Gifu University in Japan. Her research interests include computer-aided-diagnosis (CAD), image processing and image analysis, discriminant analysis, statistics in relation to CAD systems and evaluations.

Ryujiro Yokoyama received the PhD in Graduate School of Medicine from Gifu University, Japan in 2007. He is also a radiological technologist and working in Gifu University Hospital from 1976 till now. His research interests include medical image processing and pattern recognition.

Masayuki Kanematsu received MD degree and PhD degree at Gifu University in 1995. He served as a visiting scholar at Department of Radiology, University of Pittsburgh from 1994 to 1995. He has been appointed to the associated professorship of Radiology Services at Gifu University Hospital since 2001. He was invited as a visiting full professor of Department of Radiology, University of North Carolina from 2002 to 2003.

Hiroaki Hoshi received MD degree and PhD degree at Miyazaki Medical School in 1987. He served as a visiting scholar at the Montreal Neurological Institute from 1991 to 1992. He has been appointed to the chairmanship of Department of Radiology at Gifu University School of Medicine since 1995.